General Machine Learning based approach to pulse classification for separation of Partial Discharges and Interference

Emanuele Ogliari, *Member, IEEE*, Maciej Sakwa, *Student Member, IEEE*, Jianguo Wei *Member, IEEE*, Weilin Liu, Benjamin Schubert, Mauro Palo.

***Abstract*— This paper describes a complete approach to filtering Partial Discharge (PD) pulses from interference in High Voltage electrical equipment using supervised Machine Learning (ML) techniques. The PD signals are registered in Ultra High Frequency radiation band with a multisensor acquisition system composed of 4 antennae. The proposed methodology focuses on the implementation ML algorithms and proposes a novel in this field approach to the onset detection of incoming signals. The goal was to achieve high accuracy of filtering with reasonably low compilation times of the ML classifier. That would allow to use the model on *edge sensor* devices.**

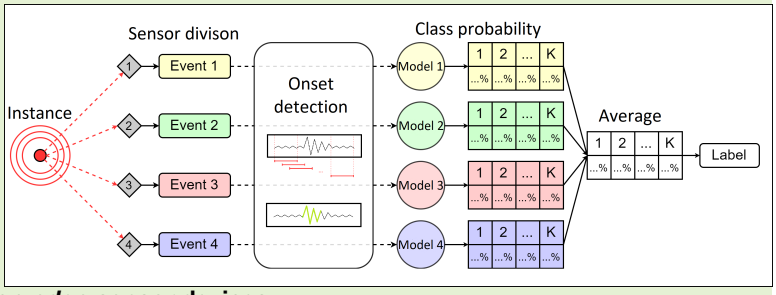

In the paper, different models and training variants of the ML framework are tested. The presented results are based on a robust measurement campaign performed in laboratories of GEIRI Europe. The methodology is validated through tests on 3 separate test scenarios. Each represents a different complexity of the problem with an increasing number of active sources. The results show high potential for utilization of the ANN and other classifiers for PD filtering problems as the accuracy achieves the desired threshold of 80% for most of the tested variants. The methodology is a step forward toward a fully online PD and interference filter.

***Index Terms*— Machine Learning, Neural Network, Onset detection, Partial Discharge**

I. Introduction

PARTIAL Discharges (PD) are localized electric discharges that only partially bridge the insulation between conductors [1] affecting only a small part of the dielectric media [2] that take place in all types of insulation systems. PD consist of self-sustaining electron avalanches caused by a local increase in field strength or a local reduction in electric strength [1], [3]. PD produce transient electrical pulses lasting around 0.1-1 μs with a pulse rise time in the range of a few ns [4] and they usually do not impact the short-term dielectric strength.

However, in the case of frequent and repetitive discharge impulses present in AC voltage, PD lead to a drastically reduced service life of High Voltage (HV) equipment [2]. Therefore, there is a constant need to monitor the PD as their occurrence is an important criterion for the evaluation of insulation quality [1]–[3].

Three main types of PD defects can be defined: internal PD, surface PD, and corona PD. Each type has different characteristics and impacts on the dielectric [5], with internal being the most damaging and corona being almost harmless to the internal structure of the insulation [6]. Due to their nature, they depend on the voltage in different ways, as can be observed on Phase-Related PD patterns (PRPD) [7]. Apart from phase-related identification, PD can be also described in the time and frequency domains. This approach allows for direct analysis of individual PD pulses and observations of the correlations between the pulses' shapes and parameters and their origin [8]. Moreover, the time and frequency pulse shape features (such as equivalent time and bandwidth) and have been previously successfully used to identify PD sources in various HV machines [9].

Traditionally the PD measurement was an operation that was conducted offline [10] using a variety of processes that accompanied a PD, such as charge displacement, emitted radiation, heat generation, acoustic emission or chemical reactions [11]. The dielectric had to be removed from the operating HV machine (e.g. a transformer) and studied in circuits designed for PD detection [2]. These methods allow for detailed analysis and description of the PD events occurring in the insulation

E. Ogliari and M. Sakwa are with Politecnico di Milano, Department of Energy, Via Lambruschini 4 - 20156 - Milano, Italy (email: emanuelegiovanni.ogliari, maciej.sakwa@mail.polimi.it

J. Wei, W. Liu, B. Schubert are with Global Energy Interconnections Research Institute Europe GmbH. Kantstr. 162 - 10623 - Berlin, Germany (email: jianguo.wei, weilin.liu, benjamin.schubert@geiri.eu)

M. Palo is with Universita degli Studi di Napoli Federico II, Dipartamento di Fisica, Via Cinthia, 21 - 80126 - Napoli, Italy (email: mauro.palo@unina.it)

[12] and are generally considered noise-free compared to the online counterparts [13].

The need to examine PD during the machine operation [14] led to the development of various methods implementing techniques such as electromagnetic or acoustic waveform monitoring. The conventional acoustic method is usually prone to suffer from various electromagnetic interference issues related to the measurement device (even though the typical frequency for acoustic PD detection is 20kHz to 300kHz). Yet, recent developments show a high potential of adapting this technology with the use of optical fiber-based sensors to achieve better results in condition monitoring of HV equipment [15].

PD pulses can occur in the region of about 600 MHz to 2 GHz [2], therefore in online measurements Very High Frequency and Ultra High Frequency (VHF/UHF) band recordings with a very high sampling rate are currently the most widely used and studied [16], [17]. The VHF/UHF band measurement has proven to be relatively noise-free in comparison to other online PD measurement methods [18], especially with additional denoising applied [19], and allows for reliable and early detection of defects in various HV machinery, such as Gas Insulated Switchgear [17], [20] and HV transformers [16], [21]. However, the radio-frequency bandwidth is relatively crowded (due to e.g. mobile phones) and it is necessary to filter out the incoming PD signals from interference present in the same bandwidth [22] in a real-life environment.

II. Machine Learning in PD detection

With recent advancements in Machine Learning (ML) techniques, there has been a noted growth in approaches to handle PD pulses with new or existing algorithms [23]. The uses range from attempts to denoise the recorded PD signal [24] with Neural Networks (NN), to the localization of PD defects [25], and the classification of PD pulses with regard to the emitting source (a different defect or an interfering factor) [23].

PD classification is a complex task, without a single correct solution, and various implementations of ML techniques and PD descriptions are proposed. Artificial Neural Networks have been tested with good results with classification methodologies that focus mostly on pattern recognition within the PRPD [26], [27] and its statistical features [28], [29]. Approaches using the time-domain recording to classify individual pulses have also been made with the pulse statistical and waveform features [30], [31] or using various dimensionality reduction techniques, such as PCA [32]. In [33], [34] combined approaches have also been tested.

Other ML techniques have been also utilized for classification with good results, including Decision Tree Ensemble [35], [36], and Support Vector Machine [37], [38]. In recent years, also Deep Learning (DL) techniques have been tried. The typical uses range from the classification of PD pulses via Pattern Recognition with Convolutional Neural Networks [39] and Long Short Term Memory NN [40], to data augmentation techniques with Generative Adversarial Networks [41].

However, due to the inherent black-box design their implementation is limited the designer wants to have more control over the input features and the output [23]. Moreover, DL techniques suffer greatly when the availability of the training data is low, and the computational burden of both classification and training is high [42]. Due to our desired use as a universal filter installed on programmable hardware (as an *edge computing* smart sensor) we decided to use the standard ML techniques in our work [43]. With further development of the computational capacity of small controllers the switch to DL will become highly reasonable [44].

This work proposes and tests a complete classification methodology starting from the signal acquisition sensors and their setup, continuing with the data transformation pipelines, and finishing with an ML classification algorithm test. The proposed method allows for the identification and filtering of individual VHF/UHF pulses before their arrival into the recording system. The proposed methodology is desired for generic use with real-life online HV equipment. It uses supervised ML techniques and proposes a novel approach to dimensionality reduction of the incoming signals with precise detection of the pulses' onset. This approach moreover allows for better comparison of the PD-like pulses in light of their varied time-of-arrival to the four acquisition sensors.

The test is performed on a detailed dataset of VHF/UHF bandwidth pulses recorded specifically for this purpose in a remote sensing laboratory belonging to Global Energy Interconnection Research Institute (GEIRI) Europe.

In section III the main measurement procedure is described with details about the devices used to generate the pulses, later section IV contains a short description of the proposed Machine Learning (ML) approach used in the classification procedure. Sections V, VI, and VII describe in detail the data recorded in this case study and the results achieved by the implementation of the proposed methodology.

III. Measurement

The datasets were acquired via a UHF/VHF PD detection system. We conducted a detailed measurement campaign with physical sources of PD pulses and interference. The same acquisition system has been used to record pulses in other case studied including real-life situations [22], [31], [45], [46].

The acquisition system is composed of 4 bi-conical ultra-wide antennae that were installed close to potential PD sources. The pulses have been recorded through a Field Programmable Gate Array (FGPA) as short snapshots with time duration of 4μs at a sampling frequency equal to 2.5 GHz. Activation of the recording software is triggered by a quick increase in the VHF/UHF radiation spectrum on a time scale of 0.1-1μs. The bandwidth of the used bi-conical antenna is between 20 MHz-1 GHz which is sufficient to cover the bandwidth of the captures PD pulses (which for AC range between 600 MHz to 2 GHz as described in sec. I).

Generally, the antennae layout is modified depending on the studied PD source to achieve the best possible performance. In case of the measurements presented in this paper, the layout has been kept constant throughout the experiments. The goal was to place the PD source somewhere in the middle of the antennae setup with all sensors at a distance of 1-2 meters from the emitting source. The measurement setup is presented

in Fig. 1 and the exact location of the sensors and PD sources is shown on the top view in Fig. 2.

Fig. 1: Measurement setup in GEIRI Europe laboratory, Berlin, Germany.

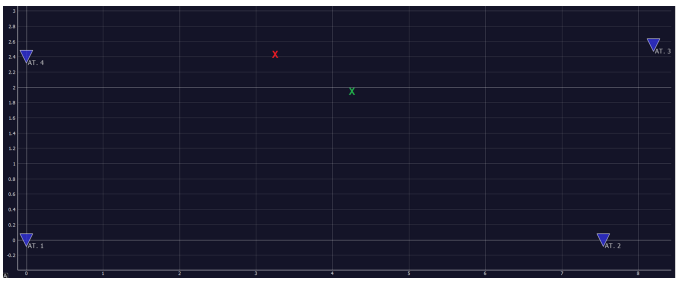

Fig. 2: Antennae layout used in the experiment - green X marks the location of the PD device, green - APG, ARC location has not been tracked thoroughly.

The PD-pulse generation has been achieved using a portable *PDSIM-600* model device by Spark Instruments that is able to physically emulate 6 different kinds of insulation defects and related PD pulses (as seen in Fig. 3 (a), the nameplate with more details in Fig. 3 (b)). The device is commercially available and the authors did not participate in its design. In the recording of the dataset the sources have been activated individually, (apart from a few test setups described in more detail later) by stimulation with AC voltage equal to 5 KV. This allowed for clear representation of the studied sources both in form of the acquired UHF waveform and PRPD for each source.

Moreover, to simulate background conditions and test the ML-based filter, other devices have been used that generate interference at the same bandwidth as the PD signals (as seen on Fig. 4). The two devices used for that purpose where an electric arc lighter (ARC) that emits chaotic signals with respect to their phase and power spectra and an artificial pulse generator (APG) designed by the authors that can emit pulses in strict power and phase range that can be set during the measurement.

All the recorded pulses (PD defects and the recorded interference) are presented in their time and frequency domain representation in Fig. 5 (based on a single example from the relative recorded dataset), and the collection of their PRPD patterns is shown in Fig. 6. A PRPD graph contains the

(a)

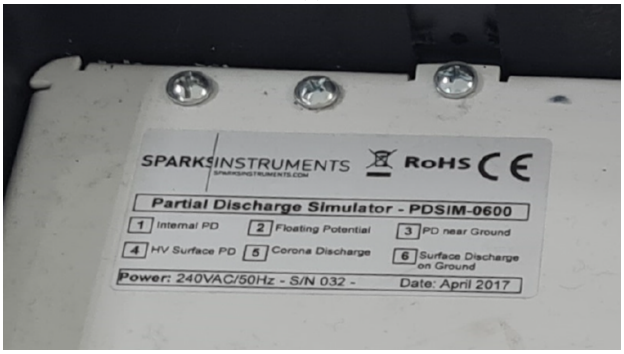

(b)

Fig. 3: PDSIM-600 device (a) the device, (b) zoom at the nameplate

(a) (b)

Fig. 4: Interference generation devices (a) ARC, (b) APG.

scaled power of all single pulses (in dB) associated with each cluster represented as a function of the 50 Hz power cycle. These graphs allow for visual Pattern Recognition (PR) of the recorded signals and will be used to distinguish the *PD* clusters from the *Noise* clusters.

As can be seen in Fig. 5 and Fig. 6 it is quite easy for the human eye to notice the differences between PD pulses and interference. In the time domain, PD signals are usually characterized by a short but dense fluctuation in the UHF waveform with fairly low power (as the background noise is still relevant in those cases). However, the difference is even more visible on the PRPD. PD pulses have a strong correlation with phase as the events are usually located in the rising part

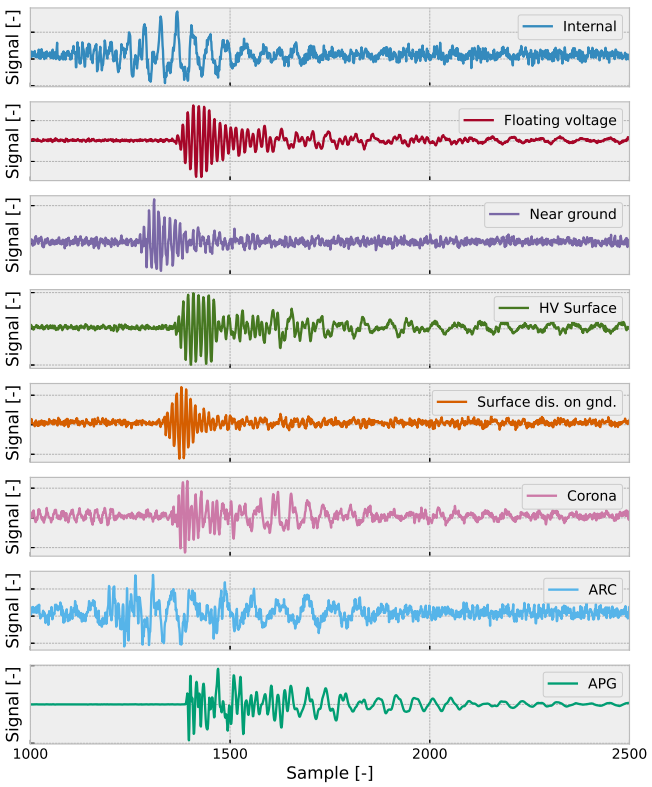

(a) Time domain

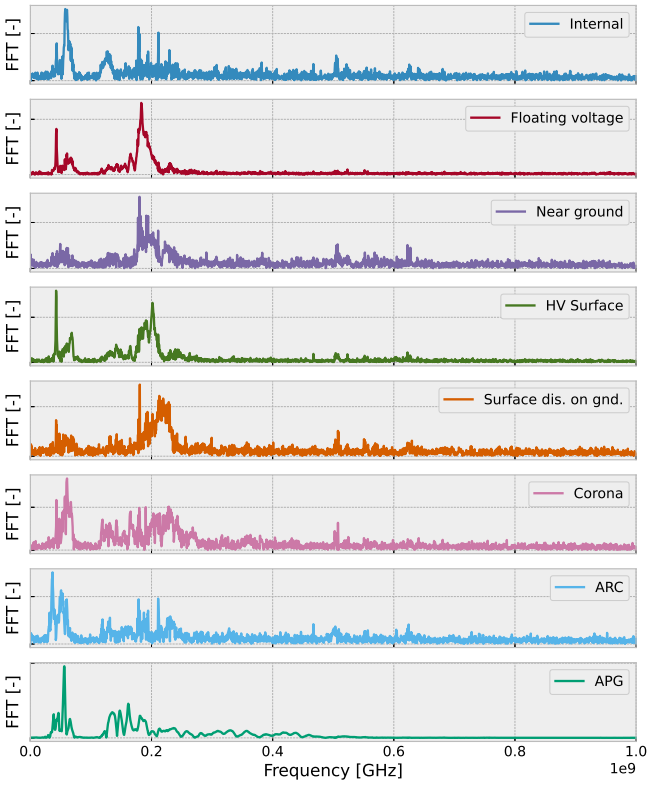

(b)

Fig. 5: Representation of recorded UHF pulses (a) time domain, (b) frequency domain.

of both positive and negative half cycles in a stochastic power range. In comparison, the interference has either a completely random distribution when it comes to phase (ARC) or is very strongly defined in its occurrence (APG).

The proposed algorithms have been tested on a workstation at Politecnico di Milano, equipped with an Intel® Core™ i9-10900KF CPU with 10 cores of the base frequency of 3.7 GHz. Additionally, a GPU based on the Ampere architecture "Nvidia GeForce RTX 3060", supporting complex tensor operations was used. The version of CUDA drivers is 11.2 and the related TensorFlow version is 2.8.

IV. Methodology

Here we propose a fast ML methodology of multi-class and multi-sensor classification that utilizes supervised learning techniques supported by a precise signal onset detection method. The procedure can be summarised by a flowchart present in Fig. 7.

A. Onset detection

In a previous study [31], we showed that training a classification ANN model on the entire waveform as an input can lead to satisfying results. However, the original waveform of each signal has 5120 samples thus the training and classification become highly demanding for even high-end machines. We simplify the waveform by designing a feature extraction method that keeps the original waveform but significantly shortens it compared to the original recording. For that purpose, an onset detection methodology has been employed to pinpoint the precise beginning of each PD-pulse waveform. Furthermore, onset detection helps to avoid the problem of misclassification of samples due to travel lag and varied arrival times between sensors. Due to onset detection, the detection of an exact location itself becomes irrelevant for the purpose of the functioning of the filter. However, it is still relevant for the general diagnostics of the HV machinery.

The onset detection procedure is as follows:

1) A sequence of partially overlapping moving windows is identified and the mean sixth statistical moment (S_6) is computed for all the samples belonging to the window:

$$S_k = \frac{\mu_k}{\sigma^k} = \frac{E[(X-\mu)^k]}{(\sqrt{E[(X-\mu)^2)}]^{k/2}} \quad (1)$$

For k equal to 6, where X are the values from the chosen window μ and σ are respectively their mean and standard deviation, and E is the expected value. From the result the standardized cumulant is subtracted (equal to 15 for the 6-th order high-order statistic) to bring the values close to 0. Values close to 0 indicate that only mostly noise is recorded in the given time window.

2) For each window, a derivative of the S_6 is calculated (dS_6), and its maximum value is identified. A threshold is set equal to 10% of the maximum value retrieved. This threshold definition has proven to be effective for real-life case studies and lab tests.

3) All the crossings between dS_6 and the threshold are identified by checking the sign of a product of two

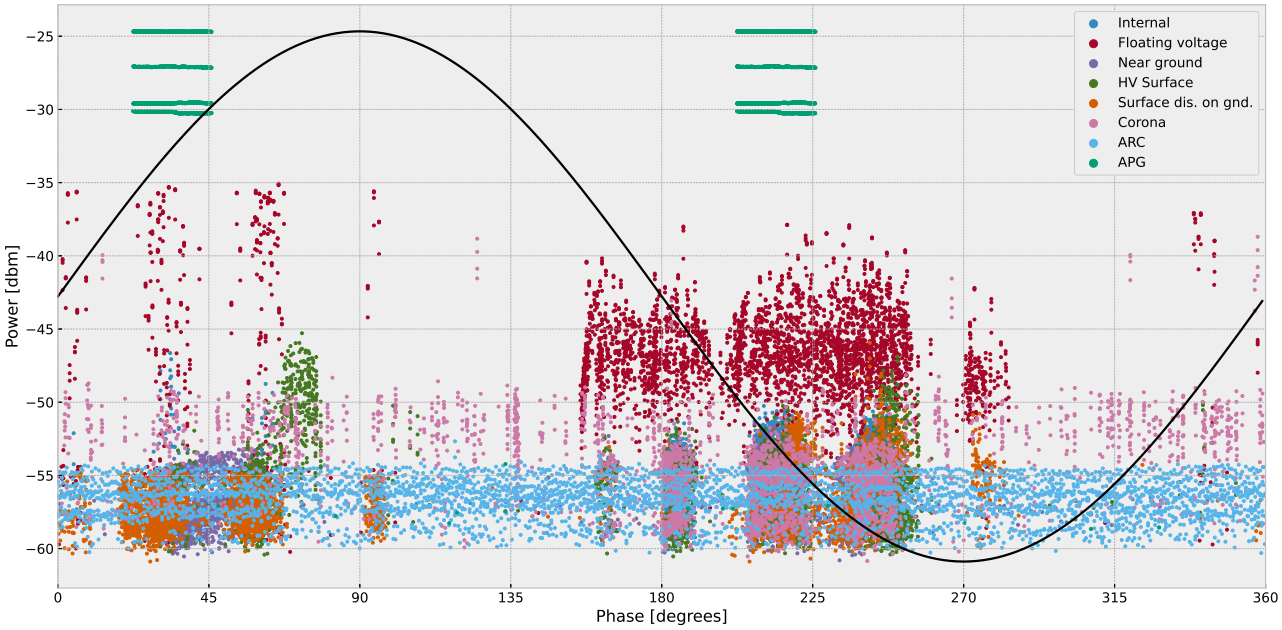

Fig. 6: Phase Related Partial Discharge pattern of all the recorded pulses used for the training of the ML interference filter. Each typology has been recorded separately by activating the sources one by one.

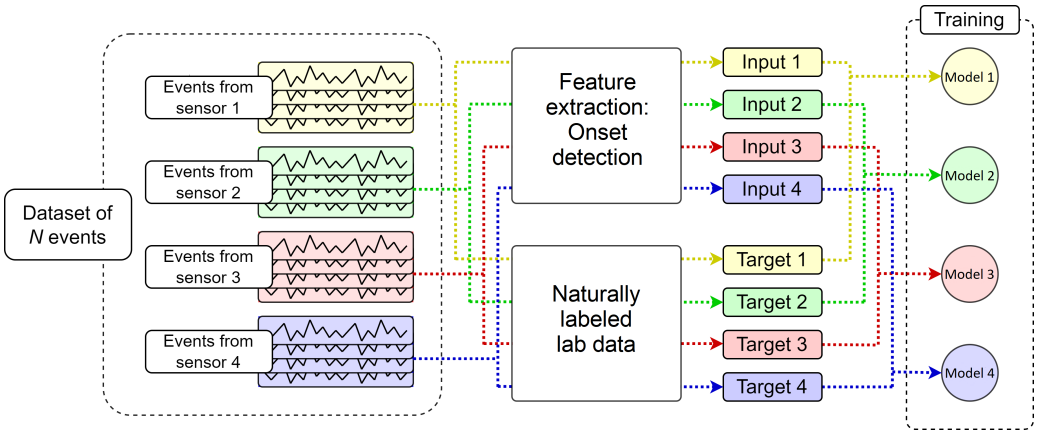

Fig. 7: Flowchart representing the training structure of the ML models. A single model corresponds to data from a single sensor.

following values of dS_6: $dS_{6,n}$ and $dS_{6,n+1}$ compared against the threshold [47].

$$C_{id,n} = sgn[(dS_{6,n} - t) \cdot (dS_{6,n+1} - t)] \quad (2)$$

Where $C_{id,n}$ is the identifying index of a given sample and t is the threshold value for the given signal. For negative values of the $C_{id,n}$ index a crossing is identified at the n-th sample of the signal.

4) For each crossing a Signal-to-Noise ratio is calculated. It is defined as a ratio of the energy content of the 250 samples (corresponds to 5% of the recorded signal) after the crossing to the energy content of the 250 samples before the crossing:

$$SNR = \frac{\sum_{i=n}^{n+250} s_i^2}{\sum_{i=n-250}^{n} s_i^2} \quad (3)$$

Where s_i is the value of the signal at the i-th sample. The crossing sample with the highest SNR value is chosen as the proper onset.

Afterward, only 12% of the original waveform is kept as a single signal of 5120 samples is reduced to 625 samples. The procedure is visualized in Fig. 8. The shortened waveforms are later used as input for the classification models.

B. Model Selection and Training

In the selection process of the model best fitted for the filtering task, we studied 5 typical classification models that are widely available in open-source packages: Support Vector Machine Classifier (SVC), Random Forest Ensemble Classifier (RFC), K-Nearest Neighbors Classifier (KNN), Gradient Boosting Classifier (GBC), and an Artificial Neural Network Classifier (ANN). The preliminary hypothesis (according to

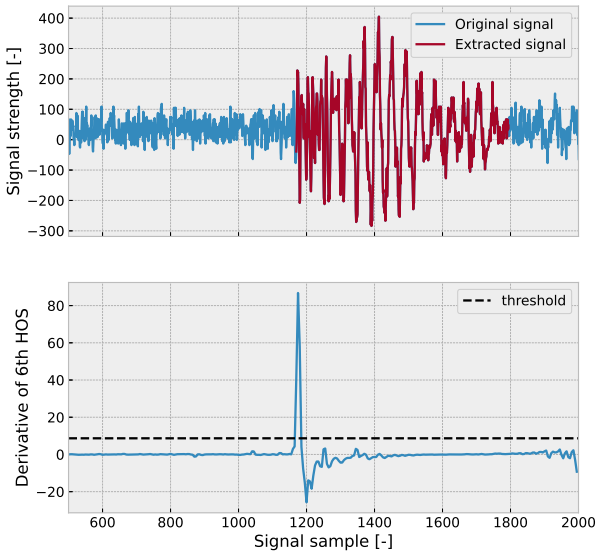

Fig. 8: An example of the pulse onset detection based on the derivative of the sixth order statistic moment (dS6). The result is the shortened waveform (in burgundy).

previously performed studies in [31]) assumed the best performance for ANN, therefore the training procedure was focused on achieving the best possible parameter tuning for this classifier. Also for this reason, in the next sections of the paper, the detailed simulation results are going to be shown only for ANN. Through a short sensitivity study, the optimal parameters were picked:

- Input layer with for feature space composed of the shortened waveform (625 samples) with Rectifier Linear Unit activation function,
- Two hidden layers with 50 neurons each with Rectifier Linear Unit activation function,
- Output layer with a shape adapted to the number of classes with ”softmax” activation function.

The rest of the classifiers are considered a benchmark in this case study. Their parameters are tuned through a brute-force style grid search in order to achieve the best accuracy score on the validation dataset. Each model (ANN included) is trained through 5-fold k-fold cross-validation with stratified shares of the training data. Finally, the optimal models are kept and tested in the later part of the paper. In each case, the model training input is composed of defined input-label pairs, with shortened waveforms (625 samples each) serving as the input and recording ID being the label. In this case, the input waveforms are not standardized or scaled, as the strength of the signal also carries information about the emitting source.

In reality, for each case, 4 separate models are trained, with one model per acquisition sensor (as shown in Fig. 7) This was done to achieve classification based on the emitted source instance, even for those pulses that do not have an equal full coverage in all the sensors. In the end, the final result for each emitted instance is calculated as an average of the proposed classification probabilities, where the models that do not have their pulse representation for a given emitted instance are ignored in the process.

V. Case study

A. Training dataset

The case study is based on the data recorded during experiments in laboratories belonging to Global Energy Interconnection Research Institute Europe GmbH (GEIRI Europe) in Berlin, Germany. The recorded data can be subdivided into two parts that were separately used for training and testing of the developed ML filtering procedure.

The training dataset has been prepared by separate activation of the available emitting sources (as already introduced in section III) - 6 PD signals from PDSIM-600 emulator and 2 interference sources. The interference has been particularly chosen to represent different repetition rates of the signal (for ARC order of magnitude of 1-10 kHz, and for APG - 100 Hz). During a single source activation, the acquisition system has been kept online until 4000 events have been recorded. As a result, a library of 32000 perfectly labeled signals (due to separate recording) has been obtained. All the recorded sources with corresponding IDs are listed in Tab. I.

TABLE I
Recorded defects and interference

ID	Defect type	Type
1	Internal PD	PD-like
2	Floating voltage PD	PD-like
3	Near ground PD	PD-like
4	HV Surface PD	PD-like
5	Corona PD	PD-like and interference
6	Surface Discharge on Ground PD	PD-like
7	ARC	Interference
8	APG	Interference

The corona discharges happen on the edge (outside) of the dielectric, hence their harmfulness depends on the type of HV equipment [2]. Moreover, their presence might disturb the functioning of the acquisition and filtering system. It is especially true for open-air equipment, such as HV transformers [48], when PD acquisition systems might be triggered by corona discharges occurring in the overhead HV electric lines.

Therefore, different affiliations will be tested for the PD defect number 5, that is the *corona*. Each test case will be run with the ML model trained with the defect being treated as a PD, and later as an interference similar to ARC or APG devices.

A decision had to be made regarding a proper approach to ML model training. Many ML algorithms (such as SVC) can perform worse in cases of multi-class classification, especially with a high amount of possible classes and a low amount of class member samples. For that reason, both multi-class and binary classification will be tested and compared (the grouping procedure can be seen in Fig. 9):

1) **Multi-class classification** - each recorded source is labeled as a separate class for training purposes. Therefore, the classifier labels the test samples as belonging to one of eight available classes. For comparison purposes,

these classes are grouped a posteriori into PD-like and interference signals results according to the key from Tab. I.

2) **Binary classification** - the training datasets are grouped before training as PD-like and interference according to the key from Tab. I. In this case, the classification procedure will be performed based on two classes instead of eight.

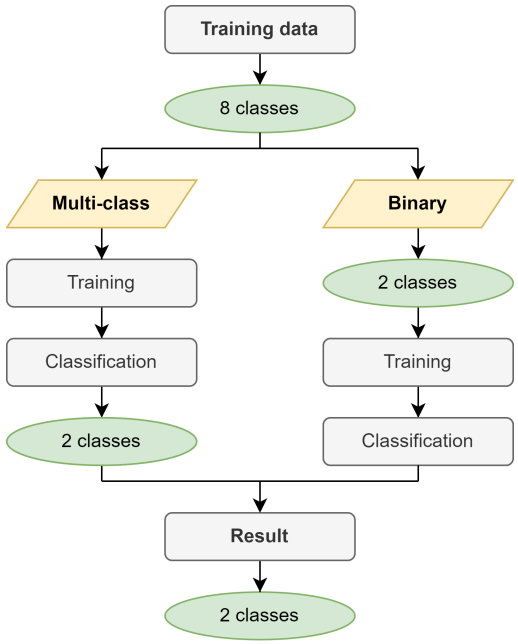

Fig. 9: Training and classification source grouping flowchart.

The *binary* training has a significant additional computational advantage in form of direct signal classification into "PD-like" and "Interference" groups. This can be particularly advantageous in achieving the edge-computing (sensoring) goal of the algorithm. The interference signals could be filtered "on the edge", before being properly recorded by the system and without clogging the data transition pipelines and involvement of human control to properly group the classes a-posteriori.

B. Test dataset

The test cases have been recorded separately from the original training dataset. In this case, each scenario uses a different combination of previously independently recorded sources. The recording has been performed similarly with the acquisition system online until a batch of 4000 signals is captured, however, here multiple sources have been activated at once. To properly test the filtering procedure the subsets were created with the inclusion of Interference signals as a "background" for PD-like pulses. As can be seen in table II in total 3 different scenarios are tested. Defects IDs are referred to the list in table I.

All of the recorded test scenarios represent the same type of defect (defect 3 - Near Ground PD) on 3 different backgrounds. It has been chosen due to its standard behavior compared to other PD defects in their time, frequency, and phase domains (as seen in Fig. 5 (a), (b), and Fig 6 respectively). The scenarios vary in complexity with more sources being introduced to the mix. In scenario I the defect is presented on its own with 2 clear interference-generating devices (ARC and APG). In scenario II the Corona defect is added as an *unclear* interference (*unclear* due to its mixed treatment as in Tab. I). Finally, scenario III adds a second clear PD pulse source (defect 1 - internal PD).

VI. Performance metrics

The proposed model will be evaluated using four metrics that are commonly used in classification problems:

- *Accuracy* - the global accuracy of the classification model and is defined as the ratio of correctly identified signals (TP total) to the total number of signals recorded:

$$Accuracy = \frac{TP_{total}}{Total\ input\ signals} \tag{4}$$

- *Precision* - the ratio of correctly identified class members (True Positive class) to the total predicted class members (True Positive plus False Positive of a class) [49]:

$$Precision_c = \frac{TP_c}{TP_c + FP_c} \tag{5}$$

- *Recall* - the ratio of correctly identified class members (True Positive class) to the total true class members (True Positive plus False Negative of a class) [49]:

$$Recall_c = \frac{TP_c}{TP_c + FN_c} \tag{6}$$

- *F1-score* - a weighted parameter combining precision and recall. For this study the weight has been considered equal [50]:

$$F1_{score} = \frac{2 \cdot Precision_c \cdot Recall_c}{Precision_c + Recall_c} \tag{7}$$

In the test cases, the "true" label of the signals is identified through a Hierarchical Agglomerative Clustering Procedure (HAC) that was previously described in [45]. It is based on a pairwise Cross-Correlation (CC) of pulses and was proven to be effective for the identification of different groups of pulses within a batch of signals.

However, this procedure does not result in the desired *PD-like* or *Interference* labels. The PRPD patterns of the resulting clusters have to be studied and, through comparison with typical individual PRPD patterns of both PD and interference, manually labeled as such. An example of this procedure can be seen in Fig. 10 where results of HAC for Scenario I are shown. These results have to be compared with the general PRPD pattern of the available sources (in Fig. 6) to identify the true labels of the defined groups. In the end, cluster 1 can be labeled as a *PD* source, due to its defined power and phase signature, while clusters 0 and 2 are labeled as *Interference* as they show similar behavior to APG and ARC respectively.

TABLE II
TEST SCENARIOS - ACTIVATED SOURCE COMPOSITION

	PD-like defects					Interferences		
ID	1	2	3	4	6	5	7	8
Type	Internal	Floating vol.	Near Ground	HV Surface	Surface-Gr.	Corona[1]	ARC	APG
I	-	-	X	-	-	-	X	X
II	-	-	X	-	-	X	X	X
III	X	-	X	-	-	X	X	X

[1] Note that PD defect Corona is considered here as "Interference" on purpose

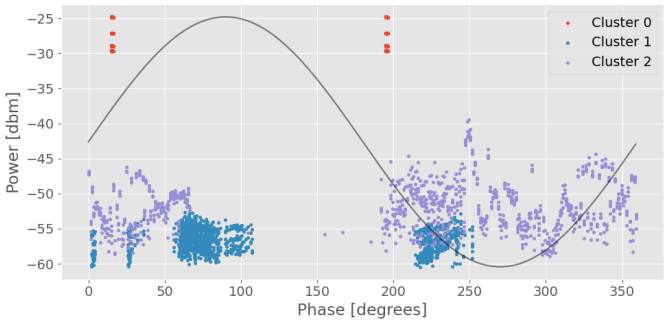

Fig. 10: CC-based HAC clusters identified in Scenario I test case; the true labels for test cases are defined based on comparison of the patterns with PRPD in Fig. 6.

VII. RESULTS AND DISCUSSION

Each of the three different test scenarios is used to find the accuracy of classification for the 5 defined classification models (SVC, RFC, KNN, GB, and ANN) trained for both binary and multiclass classification tasks. Regarding the treatment of the *Corona* discharge as interference or PD, we also tested the performance of the models in both of the specified cases. In total, 60 test cases have been performed and the general results are presented in Fig. 11, for *Corona* as PD, and in Fig. 12, for *Corona* as interference.

The main takeaway from these graphs is the fact that most of the proposed classifiers (even the simpler ones) achieve the desired accuracy of 80% (marked on graphs with the dashed line). Additionally, no matter the method used, the accuracy decreases with the increased complexity of the scenario. Generally, the *binary* training case presents higher accuracy with a very low drop in between different scenarios. Surprisingly treating *Corona* as an interference brings better stability to the model and decreases variance between scenarios. The possible explanation could come from the fact that the original training recording of *Corona* is far from perfect (as seen in Fig. 6) with numerous Interference pulses being caught in the mix. Hence, the uncertain treatment of *Corona* discharges is reflected by somewhat faulty recording. Thus, it is probably easier for the classifier to consider these pulses as *Interference* rather than PD pulses.

Aggregated results can be seen in Tab. III. With the second-best results, the hypothesis of ANN being the optimal classifier for this task can be easily questioned. However, considering the lower standard deviation of ANN in comparison to KNN (which has the best accuracy) it can be stated that ANN performance is generally more stable and thus better fitted for a multipurpose filtering tool.

TABLE III
AGGREGATED CLASSIFICATION ACCURACY

Model	Average acc.	STD acc.
SVC	87.62%	± 4.8%
RFC	85.37%	± 8.6%
KNN	89.11%	± 7.8%
GBC	87.27%	± 5.9%
ANN	88.11%	± 6.8%

A more detailed study of the ANN performance has also been conducted for the *Corona as Interference* case. Based on metrics defined in section VI, precision, recall, and F1-score have been calculated for each scenario and the results are presented in tables Tab. IV, Tab. V, and Tab. VI. The scenarios represent an increasing level of complexity, along with an increasing number of active PD and interference sources (as seen in Tab. II).

As can be seen for ANN all the results achieve the desired threshold of 80% accuracy with good values in terms of precision and recall of the *Interference* class prediction. On the contrary, for scenarios II and III the results for *PD* are not completely satisfactory with the precision and recall for the class at relatively low levels. This signifies that the filtering is too strict as many *PD* pulses have mistakenly been classified as *Interference* and rejected by the filter. This confusion is most probably caused by the inclusion of *Corona* discharge in the *Interference* group, as the ANN learns that patterns that are typically more in line with typical PD should represent one of the rejected classes.

As for scenario III, the expansion of added sources has a further impact on the detection and classification accuracy of the system. Nonetheless, the global accuracy for ANN still exceeds the desired threshold of 80%. Similarly, low precision values are observed for the *PD* class, as it reaches 63.5% and 45.8% for binary and multiclass training respectively, resulting in a high number of interference signals that are passed through the filter. Moreover, as the amount of recorded signals grows (a recording of 4000 signals is a matter of a few seconds), this outcome might be considered highly undesirable as it may lead to clogging of the data pipelines. Further studies have to be performed to optimize the precision of the *PD* class in different test cases.

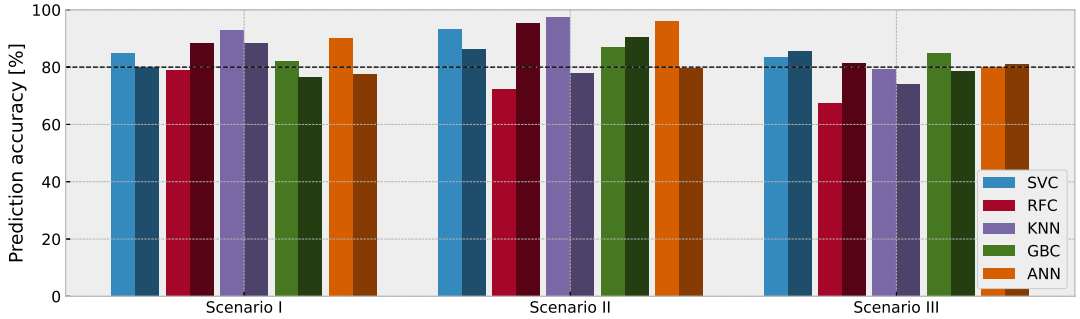

Fig. 11: Global accuracy for all the test cases for corona as PD. The lighter shade is for binary training, and darker for multi class.

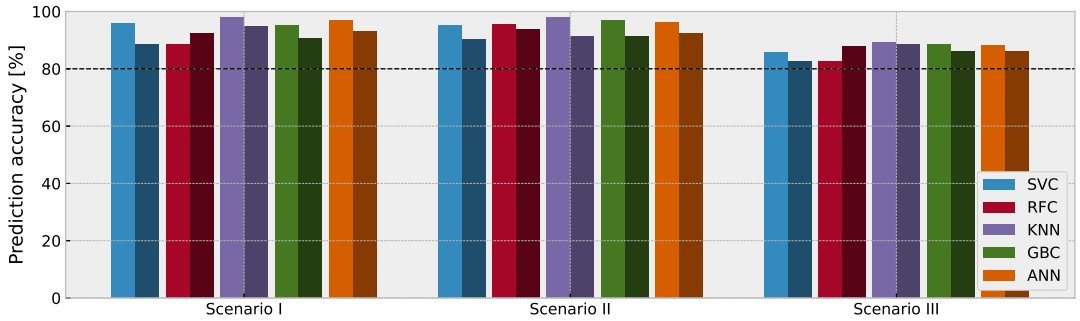

Fig. 12: Global accuracy for all the test cases for corona as interference. The lighter shade is for binary training, and darker for multi class.

TABLE IV
SCENARIO I - ANN DETAILED RESULTS

	Multiclass		*Binary*	
	PD	Inter.	PD	Inter.
Prec.	71.4%	100%	81.2%	100%
Rec.	100%	72.8%	100%	91.5%
F1.	83.3%	84.3%	89.6%	91.5%
Acc.	**93.0%**		**97.0%**	

TABLE V
SCENARIO II - ANN DETAILED RESULTS

	Multiclass		*Binary*	
	PD	Inter.	PD	Inter.
Prec.	47.6%	99.7%	88.3%	99.4%
Rec.	99.2%	69.1%	97.9%	96.3%
F1.	64.3%	81.6%	92.9%	97.8%
Acc.	**92.4%**		**96.2%**	

TABLE VI
SCENARIO III - ANN DETAILED RESULTS

	Multiclass		*Binary*	
	PD	Inter.	PD	Inter.
Prec.	62.6%	75.6%	99.6%	72.4%
Rec.	72.9%	65.9%	51.6%	99.8%
F1.	67.3%	70.4%	67.9%	83.4%
Acc.	**86.0%**		**88.17%**	

VIII. CONCLUSIONS

As demonstrated, Partial Discharge detection and classification is a complex problem that requires a robust solution that spans across various areas of expertise: from electrical engineering, through signal processing and analysis, to statistics and machine learning algorithms.

The proposed methodology tries to bridge the gaps between these domains and deliver a general and efficient tool for filtering the PD signals from interference present in UHF band. As the tests show, despite the high accuracy of classification the precision of identification of *PD* pulses suffers for more complex recordings. Further optimization of the selected model training has to be performed to decrease the number of signals that are rejected by the filter. With proper implementation, all of the tested models used in the developed procedure had good enough accuracy and compilation times to be used as an online filtering tool for *edge sensoring*.

However, a question remains on the treatment of *corona* PD pulses. As discussed, depending on the use case, it can be considered either as an *interference* or as one of the *PD* pulses. Surprisingly, the classification accuracy is slightly better and more stable when treating it as an *interference*, which might be caused by an imperfect recording for the training dataset. Additionally, the binary classifiers tend to outperform multiclass predictions by a small margin in almost every tested case.

Nonetheless, the global accuracy generally exceeded 80% for all the examined cases, thus the main goal of the performed case study has been achieved. With good accuracy and satisfying runtimes, the methodology is a step forward toward a fully online PD and interference filter.

REFERENCES

[1] Standard, "High-voltage test techniques: partial discharge measurements," *IEC-60270*, pp. 13–31, 2000.

[2] A. Kuchler, *High Voltage Engineering: Fundamentals - Technology - Applications*. Springer Link, 2018.

[3] W. Hauschild and E. Lemke, *High-voltage test and measuring techniques*. Springer, 2014, vol. 1.

[4] R. Bartnikas, "Partial discharges. their mechanism, detection and measurement," *IEEE Transactions on dielectrics and electrical insulation*, vol. 9, no. 5, pp. 763–808, 2002.

[5] R. J. Van Brunt, "Stochastic properties of partial-discharge phenomena," *IEEE Transactions on Electrical Insulation*, vol. 26, no. 5, pp. 902–948, 1991.

[6] C. Hudon and M. Belec, "Partial discharge signal interpretation for generator diagnostics," *IEEE Transactions on Dielectrics and Electrical Insulation*, vol. 12, no. 2, pp. 297–319, 2005.

[7] F. Kreuger, E. Gulski, and A. Krivda, "Classification of partial discharges," *IEEE transactions on Electrical Insulation*, vol. 28, no. 6, pp. 917–931, 1993.

[8] W. J. K. Raymond, H. A. Illias, A. H. A. Bakar, and H. Mokhlis, "Partial discharge classifications: Review of recent progress," *Measurement: Journal of the International Measurement Confederation*, vol. 68, pp. 164–181, 2015.

[9] A. Cavallini, G. C. Montanari, and F. Ciani, "Diagnosis of ehv and hv transformers through an innovative technique: Perspectives for asset management," in *Conference Record of the 2008 IEEE International Symposium on Electrical Insulation*, 2008, pp. 287–290.

[10] M. Judd, L. Yang, and I. Hunter, "Partial discharge monitoring of power transformers using uhf sensors. part i: Sensors and signal interpretation," *Electrical Insulation Magazine, IEEE*, vol. 21, pp. 5 – 14, 04 2005.

[11] L. Angrisani, P. Daponte, G. Lupò, C. Petrarca, and M. Vitelli, "Analysis of ultrawide-band detected partial discharges by means of a multiresolution digital signal-processing method," *Measurement*, vol. 27, no. 3, pp. 207–221, 2000.

[12] M. Wu, H. Cao, J. Cao, H. L. Nguyen, J. B. Gomes, and S. P. Krishnaswamy, "An overview of state-of-the-art partial discharge analysis techniques for condition monitoring," *IEEE Electrical Insulation Magazine*, vol. 31, no. 6, pp. 22–35, 2015.

[13] G. Montanari and A. Cavallini, "Partial discharge diagnostics: from apparatus monitoring to smart grid assessment," *IEEE Electrical Insulation Magazine*, vol. 29, no. 3, pp. 8–17, 2013.

[14] M. Yoshida, H. Kojima, N. Hayakawa, F. Endo, and H. Okubo, "Evaluation of uhf method for partial discharge measurement by simultaneous observation of uhf signal and current pulse waveforms," *Dielectrics and Electrical Insulation, IEEE Transactions on*, vol. 18, pp. 425 – 431, 05 2011.

[15] S. Kanakambaran, R. Sarathi, and B. Srinivasan, "Robust classification of partial discharges in transformer insulation based on acoustic emissions detected using fiber bragg gratings," *IEEE Sensors Journal*, vol. 18, no. 24, pp. 10 018–10 027, 2018.

[16] M. Hikita, S. Ohtsuka, and S. Matsumoto, "Recent trend of the partial discharge measurement technique using the uhf electromagnetic wave detection method," *IEEJ Transactions on Electrical and Electronic Engineering*, vol. 2, pp. 504 – 509, 09 2007.

[17] T. Huecker and J. Gorablenkov, "Uhf partial discharge monitoring and expert system diagnosis," *IEEE transactions on power delivery*, vol. 13, no. 4, pp. 1162–1167, 1998.

[18] S. Tenbohlen, D. Denissov, S. M. Hoek, and S. Markalous, "Partial discharge measurement in the ultra high frequency (uhf) range," *IEEE Transactions on Dielectrics and Electrical Insulation*, vol. 15, no. 6, pp. 1544–1552, 2008.

[19] G. V. R. Xavier, R. d. A. Coelho, H. S. Silva, A. J. R. Serres, E. G. da Costa, and A. S. R. Oliveira, "Partial discharge location through application of stationary discrete wavelet transform on uhf signals," *IEEE Sensors Journal*, vol. 21, no. 21, pp. 24 644–24 652, 2021.

[20] A. Darwish, S. S. Refaat, H. Abu-Rub, and H. A. Toliyat, "Pd signal propagation in gis: Ultra-high frequency detection-based modeling," *IEEE Sensors Journal*, vol. 20, no. 16, pp. 9417–9426, 2020.

[21] J. Jiang, J. Chen, J. Li, X. Yang, Y. Bie, P. Ranjan, C. Zhang, and H. Schwarz, "Partial discharge detection and diagnosis of transformer bushing based on uhf method," *IEEE Sensors Journal*, vol. 21, no. 15, pp. 16 798–16 806, 2021.

[22] M. Palo, B. Schubert, J. Wei, and W. Liu, "Clustering-based discrimination of multiple partial discharge sources: A case study," in *2019 IEEE Milan PowerTech*, 2019, pp. 1–6.

[23] S. Lu, H. Chai, A. Sahoo, and B. T. Phung, "Condition monitoring based on partial discharge diagnostics using machine learning methods: A comprehensive state-of-the-art review," *IEEE Transactions on Dielectrics and Electrical Insulation*, vol. 27, no. 6, pp. 1861–1888, 2020.

[24] A. A. Soltani and A. El-Hag, "Denoising of radio frequency partial discharge signals using artificial neural network," *Energies*, vol. 12, no. 18, 2019.

[25] E. T. Iorkyase, C. Tachtatzis, P. Lazaridis, I. A. Glover, and R. C. Atkinson, "Low-complexity wireless sensor system for partial discharge localisation," *IET Wireless Sensor Systems*, vol. 9, no. 3, pp. 158–165, 2019.

[26] L. S. Lumba, U. Khayam, and R. Maulana, "Design of pattern recognition application of partial discharge signals using artificial neural networks," in *2019 International Conference on Electrical Engineering and Informatics (ICEEI)*, 2019, pp. 239–243.

[27] H. Herath, J. Kumara, M. Fernando, K. Bandara, and I. Serina, "Comparison of supervised machine learning techniques for pd classification in generator insulation," in *2017 IEEE International Conference on Industrial and Information Systems (ICIIS)*, 2017, pp. 1–6.

[28] A. A. Mas'ud, B. G. Stewart, and S. G. McMeekin, "An investigative study into the sensitivity of different partial discharge $\phi - q - n$ pattern resolution sizes on statistical neural network pattern classification," *Measurement*, vol. 92, pp. 497–507, 2016.

[29] A. A. Mas'ud, J. A. Ardila-Rey, R. Albarracín, and F. Muhammad-Sukki, "An ensemble-boosting algorithm for classifying partial discharge defects in electrical assets," *Machines*, vol. 5, no. 3, 2017.

[30] Y. Khan, "Partial discharge pattern analysis using pca and back-propagation artificial neural network for the estimation of size and position of metallic particle adhering to spacer in gis," *Electrical Engineering*, vol. 98, no. 1, pp. 29–42, Mar 2016.

[31] A. Matteri, M. Palo, E. Ogliari, B. Schubert, J. Wei, K. Gu, and W. Liu, "Separation of radio-frequency signals triggered by valve switching in a hvdc converter by supervised machine learning methods," in *2021 IEEE International Conference on Environment and Electrical Engineering and 2021 IEEE Industrial and Commercial Power Systems Europe (EEEIC / ICPS Europe)*, 2021, pp. 1–6.

[32] A. Dobrzycki, S. Mikulski, and W. Opydo, "Using ann and svm for the detection of acoustic emission signals accompanying epoxy resin electrical treeing," *Applied Sciences*, vol. 9, no. 8, p. 1523, 2019.

[33] T. R. Sukma, U. Khayam, Suwarno, R. Sugawara, H. Yoshikawa, M. Kozako, M. Hikita, O. Eda, M. Otsuka, H. Kaneko, and Y. Shiina, "Classification of partial discharge sources using waveform parameters and phase-resolved partial discharge pattern as input for the artificial neural network," in *2018 Condition Monitoring and Diagnosis (CMD)*, 2018, pp. 1–6.

[34] L. Li, J. Tang, and Y. Liu, "Partial discharge recognition in gas insulated switchgear based on multi-information fusion," *IEEE Transactions on Dielectrics and Electrical Insulation*, vol. 22, no. 2, pp. 1080–1087, 2015.

[35] R. Hussein, K. B. Shaban, and A. H. El-Hag, "Robust feature extraction and classification of acoustic partial discharge signals corrupted with noise," *IEEE Transactions on Instrumentation and Measurement*, vol. 66, no. 3, pp. 405–413, 2017.

[36] W. L. Woon, A. El-Hag, and M. Harbaji, "Machine learning techniques for robust classification of partial discharges in oil–paper insulation systems," *IET Science, Measurement & Technology*, vol. 10, no. 3, pp. 221–227, 2016.

[37] B. A. Desai, R. Sarathi, J. Xavier, and A. Senugupta, "Partial discharge source classification using time-frequency transformation," in *2018 IEEE 13th International Conference on Industrial and Information Systems (ICIIS)*, 2018, pp. 362–366.

[38] M. Kunicki and D. Wotzka, "A classification method for select defects in power transformers based on the acoustic signals," *Sensors*, vol. 19, no. 23, p. 5212, 2019.

[39] G. Li, M. Rong, X. Wang, X. Li, and Y. Li, "Partial discharge patterns recognition with deep convolutional neural networks," in *2016 International Conference on Condition Monitoring and Diagnosis (CMD)*, 2016, pp. 324–327.

[40] X. Zhou, X. Wu, P. Ding, X. Li, N. He, G. Zhang, and X. Zhang, "Research on transformer partial discharge uhf pattern recognition based on cnn-lstm," *Energies*, vol. 13, no. 1, 2020.
[41] W. Yijiang, L. Chen, W. Ganjun, P. Xiaosheng, L. Taiwei, and Z. Yunzheng, "Partial discharge data augmentation of high voltage cables based on the variable noise superposition and generative adversarial network," in *2018 International Conference on Power System Technology (POWERCON)*, 2018, pp. 3855–3859.
[42] I. Goodfellow, Y. Bengio, and A. Courville, *Deep learning*. MIT press, 2016.
[43] C. Gianoglio, F. Guastavino, E. Ragusa, A. Bruzzone, and E. Torello, "Hardware friendly neural network for the pd classification," in *2018 IEEE Conference on Electrical Insulation and Dielectric Phenomena (CEIDP)*, 2018, pp. 538–541.
[44] S. S. Saha, S. S. Sandha, and M. Srivastava, "Machine learning for microcontroller-class hardware: A review," *IEEE Sensors Journal*, vol. 22, no. 22, pp. 21 362–21 390, 2022.
[45] M. Palo, B. Schubert, E. Ogliari, J. Wei, K. Gu, and W. Liu, "Detection, features extraction and classification of radio-frequency pulses in a high-voltage power substation: Results from a measurement campaign," in *2020 IEEE 3rd International Conference on Dielectrics (ICD)*. IEEE, 2020, pp. 677–680.
[46] B. Schubert, J. Wei, C. P. Beura, W. Liu, and M. Beltle, "Uhf-based measurement of partial discharge in an oil-filled tank from outside," in *VDE High Voltage Technology; 4. ETG-Symposium*, 2022, pp. 1–5.
[47] F. Piñal-Moctezuma, M. Delgado-Prieto, and L. Romeral-Martínez, "An acoustic emission activity detection method based on short-term waveform features: Application to metallic components under uniaxial tensile test," *Mechanical Systems and Signal Processing*, vol. 142, p. 106753, 2020.
[48] A. Cavallini, X. Chen, G. C. Montanari, and F. Ciani, "Diagnosis of ehv and hv transformers through an innovative partial-discharge-based technique," *IEEE Transactions on Power Delivery*, vol. 25, no. 2, pp. 814–824, 2010.
[49] J. Makhoul, F. Kubala, R. Schwartz, R. Weischedel *et al.*, "Performance measures for information extraction," in *Proceedings of DARPA broadcast news workshop*, vol. 249. Herndon, VA, 1999, p. 252.
[50] Y. Sasaki *et al.*, "The truth of the f-measure," *Teach tutor mater*, vol. 1, no. 5, pp. 1–5, 2007.

Emanuele Giovanni Carlo Ogliari (M'20) is Associate Professor at the Department of Energy, Politecnico di Milano, Italy where he teaches Electrical Engineering and Photovoltaic-based Systems Lab. He has a M.Sc. in electrical engineering, and he received the Ph.D. degree in electrical engineering from the Politecnico di Milano, Italy, in 2016. He is staff member of the Solar Tech Lab (SolarTech^{LAB}) and the Laboratory of MicroGrids (MG^{2}LAB) at the same university. He has been working on photovoltaic power plant design and their optimization since 2010 and RES expected power by means of computational intelligence techniques since 2012.

Maciej Sakwa (GS'22) is a research fellow at the Department of Energy, Politecnico di Milano. He has an M.Sc. in energy engineering received at Politecnico di Milano, Italy, in 2022. Freshly graduated he now works in research fields related to Renewable Energy Sources and implementation of modern computational intelligence algorithms.

Weilin Liu Is chief scientist for cyber physic systems at Global Energy Interconnection Research Institute in Berlin Germany. He received Dipl. Ing. from Technical University Munich and Ph.D. in communications engineering from University of Federal Armed Forces Munich. He has worked mainly on various digital communication technologies. Since 2016 he has been working on sensing, signal processing and data analysis technology for power grid monitoring, with focus on the detection and localisation of Partial discharge signal in VHF/UHF frequency band.

Jianquo Wei (M'20) is senior research engineer for intelligent sensing and measurement at Global Energy Interconnection Research Institute in Berlin Germany. He has a M.Sc. in electronic and information engineering, and he received the Ph.D. degree in electronic and information engineering from the Universidad Politécnica de Madrid, Spain, in 2015. He has worked on OS-level power management and network protocols for portable and IoT devices. Since 2017 he has been working on sensing, signal processing and data analysis technology for power grid monitoring, with focus on the detection and localisation of partial discharge signal in VHF/UHF frequency band.

Benjamin Schubert is senior research engineer at the department of intelligent sensing and measurement at the Global Energy Interconnection Research Institute in Berlin, Germany. He received the Dipl.-Ing. degree in electrical engineering from the Technical University Berlin, Germany, in 2006 and then joined the department of Wireless Communication and Networks at the Fraunhofer Heinrich Hertz Institute (HHI) in Berlin, where he focused on the research topics nonlinear system modelling and RF impairment mitigation. Since 2016 he has been developing the sensing and signal processing parts of a monitoring platform for the UHF-based detection of Partial Discharge in high-voltage plants.

Mauro Palo is senior Assistant Professor at the Department of Physics "Ettore Pancini" of University of Naples "Federico II", Italy. He teaches Electromagnetism at the Faculty of Management Engineering of the University of Naples "Federico II". He has a M.Sc. in physics, and he received the Ph.D. degree in physics from the University of Salerno, Italy, in 2008. Since 2004 he has been working on unsupervised machine-learning methods combined with geophysical techniques to study the spatiotemporal properties of the seismicity in tectonic and volcanic regions.